Unraveling the Role of Azobenzene-Based Photoswitchable Lipids in Controlling Innate Immune Response

Anastasiia Delova,[a] Aline Makhloutah,[b] Yann Bernhard,[b] Andreea Pasc,[b] Antonio Monari.[a,]*

a) Université Paris Cité and CNRS, ITODYS, F-75006 Paris, France. b) Université de Lorraine and CNRS, UMR 7053 L2CM, Nancy, France.

KEYWORDS. Photoimmunotherapy, molecular photswitches, lipid membrane, innate immune system, molecular dynamic.

ABSTRACT Controlling the activation of the innate immune response, particularly through the use of suitable visible light sources, could pave the way for the development of innovative phototimmunotherapeutic strategies. In this contribution, we investigate the effects of the E/Z isomerization on a phosphatidylserine lipid containing an isomerizable azobenzene moiety, which has recently been shown to regulate the activation of natural killer cells and the production of cytokines [*J. Am. Chem. Soc.* 2022, 144, 3863−3874]. Specifically, we examine how this isomerization affects interactions with the innate immune system's TIM-3 receptors. Using long-range molecular dynamics simulations with enhanced sampling, we demonstrate that the Z isomer leads to a shallower binding and a less pronounced rigidification of the protein compared to the E isomer and the native lipid, which explains the less pronounced activation of the immune response.

TOC GRAPHIC

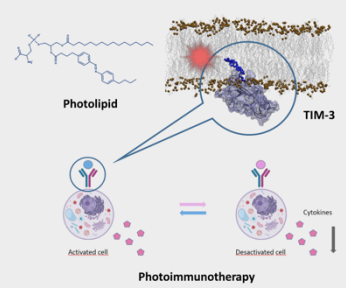

INTRODUCTION.

The innate immune system serves as the frontline defense against attacks by exogenous pathogens or endogenous agents that threaten the viability of cells and organisms.[1,2] Therefore, maintaining its proper regulation is crucial, as its dysregulation is often linked to a range of debilitating pathologies, with autoimmune diseases serving as a prime example.[3] Usually, the activation of the innate immune response triggers apoptotic signaling on one hand, leading to cell death and halting the propagation of infections.[4]. On the other hand, it stimulates the production of interferons and cytokines, which correlates with a proinflammatory response that creates an unfavorable environment for pathogens.[5,6] Different innate immune system pathways exist, which may also respond to different threats, such as the OAS/RNAse L pathways,[7–9] which is tailored to sense the presence of exogenous RNA, or the cGAS-STING[10,11] pathway, which is instead more sensitive to the presence of exogenous DNA. Recently, the role of the T cell transmembrane, Immunoglobulin, and Mucin (TIM) proteins has been particularly recognized in the regulation of the innate immune response. TIM proteins exist in different isoforms[12–14] with TIM-1, TIM-2, TIM-3, and TIM-4 being the most widely studied. They are large transmembrane proteins (Figure 1)

comprised of different domains, which include a cytosolic region, a transmembrane segment, a linker mucin domain comprising glycosylation sites,[13] and finally the N-terminal immunoglobulin–like (IgV) domain. In the case of TIM-1, TIM-3, and TIM-4 receptors, the IgV domain senses the external lipid leaflet of other cellular membranes (Figure 1B) and interacts specificallywith lipids whose polar head contains phosphatidylserine (PDS) moieties.[12,15–19] This specificity is at the base of their action, characterizing them as efficient sensors of apoptotic cells[20–28] since that during apoptosis PDS-containing lipids migrate from the inner to the outer leaflet of the cellular membrane.[22,27]

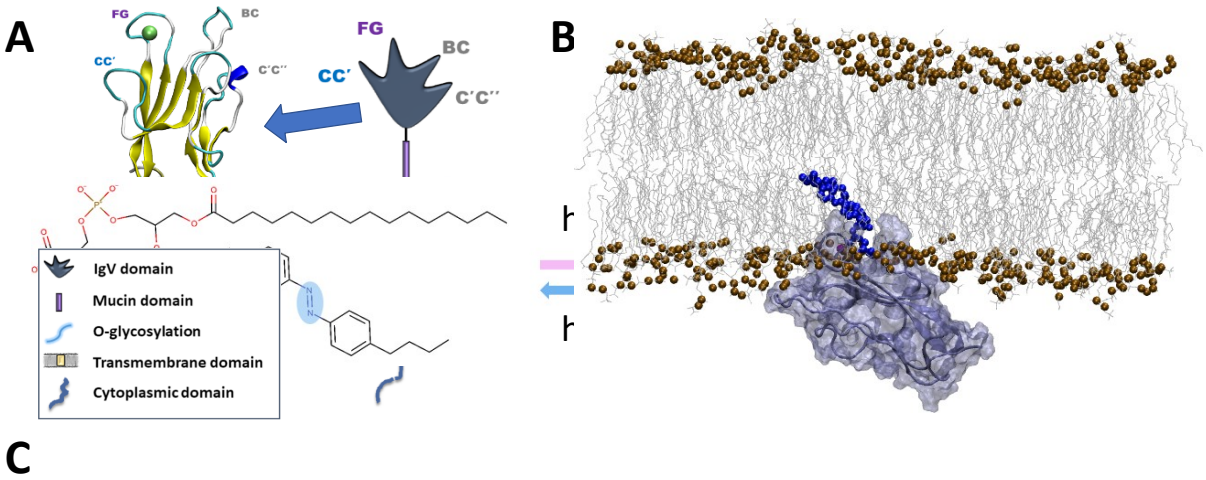

Figure 1. Schematic structure of TIM-3 highlighting the IvG domain at atomic recognition (A). Snapshot extracted from the MD simulation and showing the interaction of the IvG domain with a lipid membrane and its binding to a PDS-containing lipid (B). Representation of the E and Z isomers of the photoswitchable lipids used in this study (C).

In contrast with the other members of the family, TIM-2 does not interact with PDS and should, thus, be related to a different mechanism of actions, which remains elusive to date.[29–31] Yet the role of TIM proteins is more complex and is not restricted to the simple recognition of apoptotic cells. Indeed, a complex balance between the activation of anti-inflammatory signals, which helps in maintaining immune response tolerance, and the production of cytokine has been observed, pointing to a multifaced and highly dynamic role.[32]

TIM-3 is emerging as of particular interest among the different members of the family. It is preferentially expressed in T-helper 1 and T-cells 1,[33,34] and is also found in dendritic cells.[35] TIM-3 also represents a marker of the maturation of natural killer (NK) cells[6,29] and its activation correlates with cytokine production,[36,37] and is related to autoimmune diseases.[38] More recently, the role of TIM-3 in regulating the tumor microenvironment has been particularly pointed out.[39–42] Indeed, TIM-3 is also related to the exhaustion of T-cells in tumors or to the functionality loss of lymphocytes in the tumor microenvironment. Moreover, the overexpression of TIM-3 may be considered as a cancer biomarker, correlating with a bad prognosis,[43–45] while the blockade of TIM-3 activity has shown beneficial effects, even for the treatment of tumors in advanced stages.[46–48] Structurally the IvG domain is composed of a rigid core, rich in β barrel motifs, flanked by four flexible loops. Notably the pocket between the FG and CC' loops constitute the PDS binding site (Figure 1A).[49,50] The interaction with the phosphatidylserine is mediated by a Ca^{2+} ion and by persistent hydrogen bonds with protein residues, notably D102, Q43, and S42.[49] Recently, by using enhanced sampling and extended Molecular Dynamics (MD) simulations the thermodynamic parameters of the interaction between the IvG domain and PDS containing lipids have also been determined.[16] Notably, we have shown that the inclusion of the lipid in the binding pocket is barrierless and favored by a free energy driving force of about 15-20 kcal/mol.[16] While the polar

head is held tight between the FG and CC' loops, the lipid tails remain globally parallel to the membrane axis and stretch away from the IvG surface.

Conversely, it has been shown that PDS-containing photoswitchable lipids (PSL) including an azobenzene moiety in one of the lipid tails (Figure 1C) may act as regulator of the activity of TIM-3.[51] Indeed, under irradiation with suitable UV/Vis light, the azobenzene undergoes a fast E/Z photoisomerization[52,53] leading to the conversion of the E-PSL to the Z-PSL isomer. While the former is competitive with the native PDS lipid for the interaction with the IvG domain and the activation of the TIM-3 response, the latter is inducing a less pronounced activation of the protein.[51] Therefore, these results pave the way to the exploitation of molecular photoswitches to enforce the light-controlled activation of the immune system response. Due to the involvement of TIM-3 in cancer development and in shaping the tumor microenvironment, this strategy may be highly suitable for photoimmunotherapy purposes. However, the molecular bases leading to the differential affinity for the two isomers, and hence the different activation of the protein, remains elusive, precluding the design of improved photoimmunotherapy agents.

In this contribution, by using MD simulations and enhanced sampling protocols, we explore the interaction of the two PSL isomers with the TIM-3 IvG domain, in presence of a realistic lipid bilayer to mimic physiologically relevant conditions. In particular, we show that the Z isomers presents a slightly less favorable interaction with the protein, inducing a less pronounced rigidification of the protein scaffold, thus justifying its weaker activation.

COMPUTATIONAL METHODOLOGY

The initial structures of the PSL in E and Z conformations have been drawn using the Marvin Sketch chemical drawing software.[54] Afterwards, the geometry of both structures has been optimized at the B3LYP/6-31G(d) density functional theory, considering implicit water solvent

modeled with the PCM approach and using the Gaussian09 software[55]. On top of the optimized geometry, we have calculated the restrained electrostatic potential (RESP) charges using the HF/6-31G* level of theory. The antechamber utilities from AmberTools22[56] package were used to generate Generalized Amber Force Field (GAFF) parameters for both conformers. To precisely model the azobenzene unit, especially the torsion along the isomerizable double bond, we have replaced the original amber parameters with those described by S. Osella et al.[57]

CHARMM-GUI[58] program was used to build an initial model of a lipid membrane bilayer with a composition characteristic of eukaryotic cells. A mixture of lipids, including POPC, POPE, POPS, and cholesterol, was used with respective molar ratios of 30%, 25%, 15%, and 30%, placing a total of 200 lipids in each leaflet, in coherence with the strategy used in our previous work.[59] A 30 Å water buffer containing a physiological concentration of 0.15 M and K^+ and Cl^- ions was also included and added to the system. The IgV domain of murine TIM-3 protein, sourced from the PDB database (PDB: 3KAA),[60] provided the starting protein's conformation. The protein was placed in close proximity to the lipid's polar heads within the bulk water to allow lipids to interact with it. Lipids have been represented by Amber Lipid14 force field,[61] while water was described using TIP3P.[62,63] The IgV domain of TIM-3 was described using the Amber ff14SB[64] protein forcefield.

To place one PSL lipid in the IvG binding site we used a similar strategy to the one applied in our previous work.[59] Concretely, we considered IvG in interaction with a native POPS lipid extracted after 1 μs MD simulation. Since the polar head of the native lipid (phosphatidylserine) is identical to the one of PSL, we aligned the latter, either in E- or Z-conformation, with the POPS lipid using

the VMD program to obtain the two starting conformations for the MD simulations involving either E- or Z-PSL.

For the two initial systems we performed all-atom classical MD simulations using NAMD[65,66] software, followed by analysis and visualization performed with the VMD program.[67] Hydrogen mass repartition[68] was employed to allow the use of a 3.0 fs time-step in the propagation of the simulation *via* the numerical resolution of Newton equations of motion, also using Rattle and Shake algorithms.[69] For all systems minimization, thermalization and equilibration steps were performed, which involved gradually removing positional constraints on non-water heavy atoms over a 12 ns dynamics. Throughout equilibration and production simulations, a constant temperature of 300 K and a pressure of 1 atm were maintained, leading to an isothermal and isobaric (NPT) ensemble ensuring that the lipid membrane remains in its liquid phase. The Langevin thermostat[70] and barostat[71] were used to enforce temperature and pressure conservation, respectively. The production phase for both systems spanned a total simulation time of 1 μs. To analyze the stabilityof the E/Z-PSL-protein complex the root mean square deviation (RMSD)[72] and root mean square fluctuation (RMSF)[73] analyses were performed.

Umbrella Sampling (US)[74] was used to obtain the potential of mean force (PMF) for the interaction between the PSL polar head and the binding pocket comprised between the FG-CC' loop of the IgV domain. The selected collective variable for US was the distance between the center of mass of the PSL polar head and the protein binding pocket, including the Ca^{2+} ion and the four principal interacting residues:S42, Q43, Q95, and D102. A pictorial representation of the collective variable is also providedin SI. To achieve the enhanced sampling, starting from the bound state, we progressively increase the distance, leading to the lipid dissociation. The distance was increased from 3.0 to 17.0 Å with a step of 0.5 Å producing independent windows. Each US window has been propagated for 30 ns to ensure a good equilibration with a force of 22.5 kcal/(mol.Å). The final PMF profile was generated by integration of the different windows using the Weighted

Histogram Analysis Method (WHAM).[75] The distribution of the values assumed by the collective variable among the different windows is reported in SI, showing the good overlap between the windows.

RESULTS AND DISCUSSION

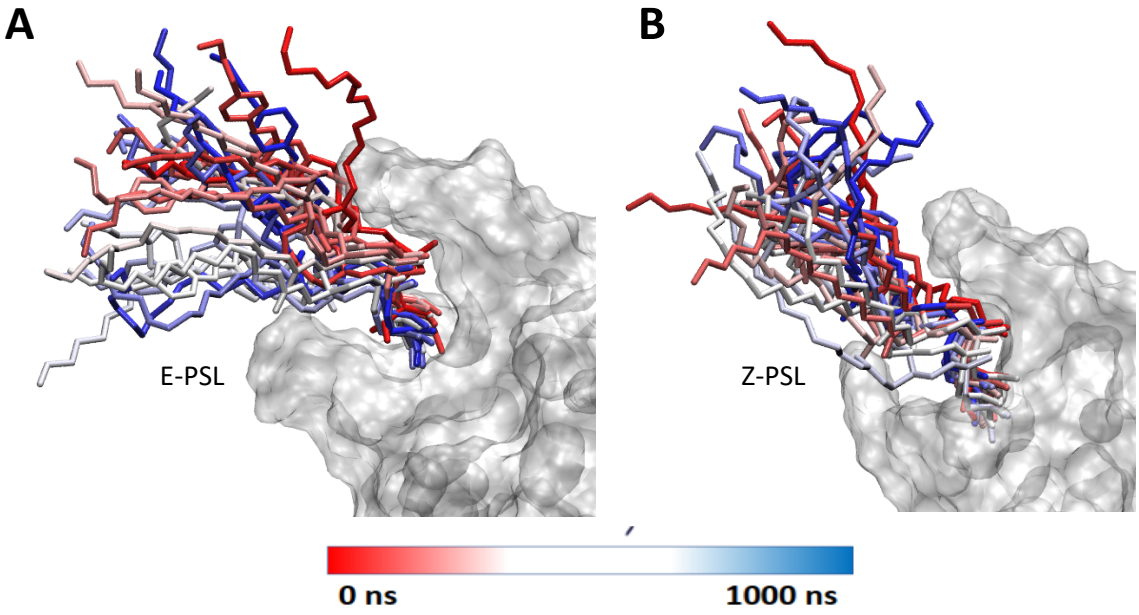

Figure 2. Snapshots showing the time evolution of the positioning of the E- and Z-PSL (panel A and B, respectively) inside the binding pocket of the IvG domain. The protein is represented as a transparent surface, while the PSL is in licorice.

MD trajectories exceeding the μs time-scale have been performed for the photoswitchable lipids interacting with the IvG binding site. Both the E- and Z-PSL isomers have shown the formation of a persistent complex with the IvG domain, remaining inside the binding pocket of the protein (Figure 2). However, the hydrophobic tails of the E isomer behave like those of native lipids, i.e. POPC moieties,[16] and extend towards the hydrophobic core of the membrane environment (Figure 2A). Instead, in the case of Z-PSL a more globular arrangement emerges inducing stronger interaction between the tails and the protein loops, which may lead to partial steric clashes (Figure

2B).

To better quantify the persistence of the interactions locking PSL into the protein binding pocket we have analyzed the main interactions between the protein residues and the lipid polar head as shown in Figure 3 and Table 1. These results are also compared to the experimental structure for an isolated phosphatidylserine moiety interacting with the IvG domain.[18]

	Native PDS (Crystal)	E-PSL	Z-PSL
Ca^{2+}	2.938	2.38 ± 0.06	2.37 ± 0.06
Q95	3.420	3.07 ± 0.42	3.62 ± 0.94
D102	2.666	2.92 ± 0.19	2.86 ± 0.16
Q43	3.084	4.63 ± 0.99	4.53 ± 1.09
S42	2.750	4.94 ± 1.20	5.13 ± 1.22

Table 1. Average values and standard deviations of the distances between the PDS unit of E- and Z-PSL and the main IvG residues in the binding pocket. The values for a reference crystal structure of a PDS unit interacting with IvG are also given as a reference.[18] The specific atoms used to calculate the distances are represented in Figure 3. All the values are given in Å

From the analysis of the average distances reported in Table 1 we may evidence no significant differences in the interaction patterns between the two isomers and the native crystal structure. Q95 shows a partial exception, in the case of the Z isomer, presenting a slightly larger average distance, as well as a more pronounced dispersion. Interestingly, this residue is located in the FG loops, which is characterized by a more pronounced interactions with the bent lipid tails in the Z isomer. In agreement with our previous results, relative to a native PDS containing lipid, we may also notice that the interaction with S42 is consistently weaker compared to the crystal structure.

This effect, which we have interpreted as due to the presence of the lipid tails missing in the reference crystal structure,[18] is also slightly more pronounced for the Z-isomer in particular considering the dispersion of the distances as also shown by the standard deviation reported in Table 1.

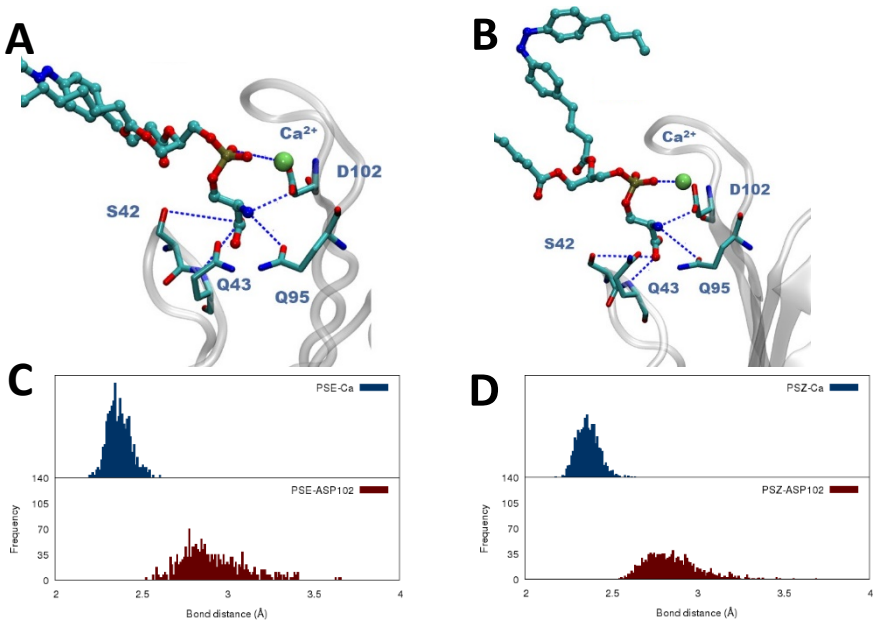

Figure 3. Representative snapshots showing the disposition of the E-PSL (A) and Z-PSL (B) in the IvG binding pocket. Distribution of the main distances along the MD simulation for the E- (C) and Z- (D) isomers, respectively.

This behavior, along with the persistence of the interaction in the IvG binding pocket, can alsobe appreciated in Figure 3, in which we may also identify the strong interaction with the Ca^{2+} ion, characterized by a sharply peaked distribution with a maximum at short distances.

Interestingly, once again these results are attuned with those obtained from the native lipid and reported in a previous contribution.[16]

Therefore, these results suggest that the E/Z isomerization of this azobenzene-based photoswitchable lipid has a relatively minor effect on the activation of TIM-3, particularly as concerns its interaction with the IgV domain.

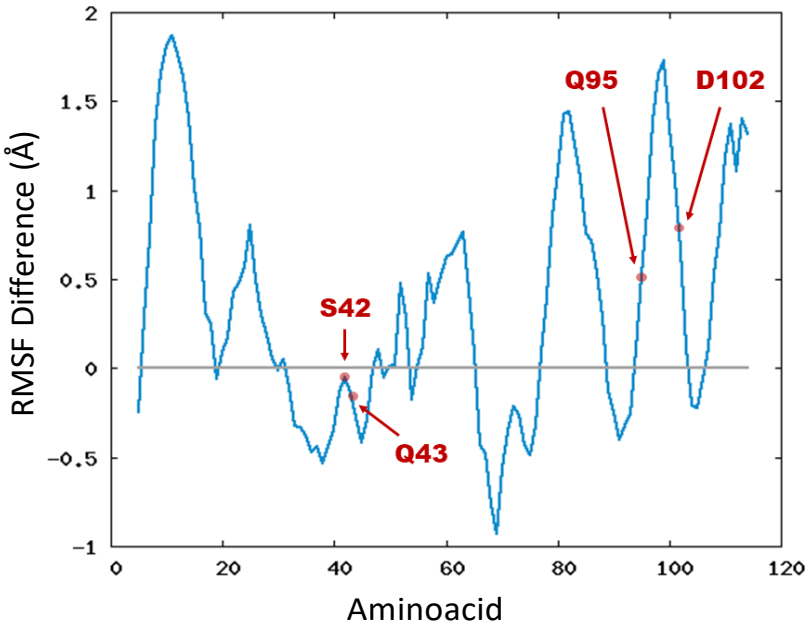

Figure 4. Difference of RMSF of the IvG domain calculated as the RMSF for the protein interacting with the Z-PSL minus the one interacting with the E-PSL. Thus, positive values indicate a greater flexibility for the Z-PSL bound system, while negative ones indicate an increase of flexibility of the E-PSL. Individual RMSF plot are provided in ESI.

However, the analysis of the RMSF plots for the IvG domain interacting with either the Z- or the E-PSL reveals significant, though moderate, differences. Indeed, in addition to the N-terminal domain, a noticeable increase of flexibility can be observed for the aminoacids belonging to the FG loop. This concerns in particular the Q95 and D102 residues which are directly located in the binding pocket and participate in the stabilization of the phosphatidylserine polar head. This effect

can be once again ascribed to the presence of the lipid tails, which in the Z isomer are susceptible to interact more strongly with the FG loop, causing partial steric clashes. Consequently, this perturbation leads to a slight weakening of the FG/PDS interactions, which ultimately results in an increased flexibility. Since TIM-3 activation also proceeds through long-range allosteric regulations triggered by the binding of PDS and transmitted to the different domains of the protein, the rigidity loss of the FG loop, in addition to the weakening of the binding, may also have a secondary effect by partially disrupting the allosteric regulations and signal transduction.

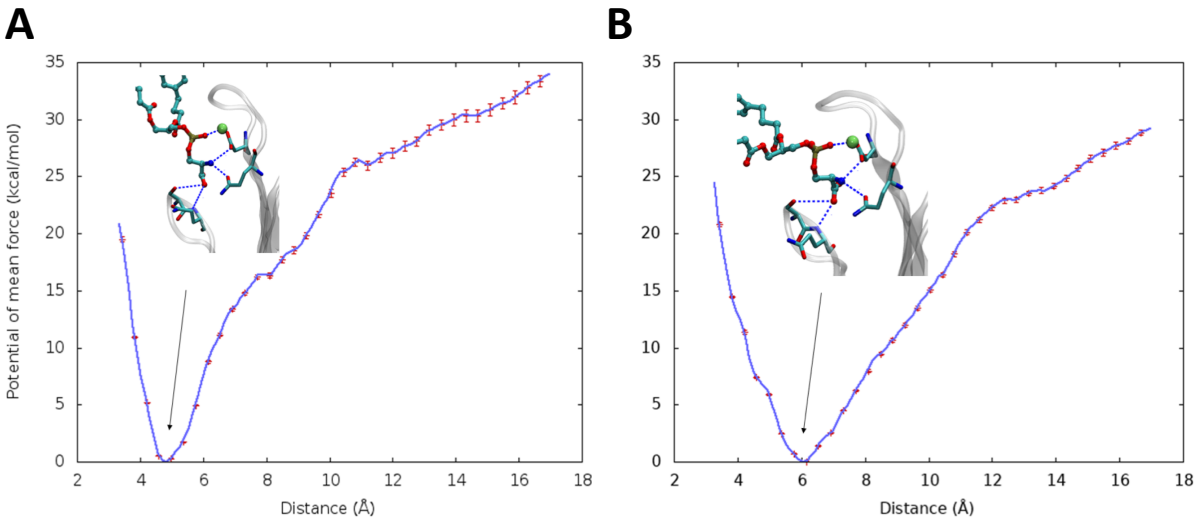

Figure 5. Potential of Mean Force profile along the distance from the binding pocket for the E-PSL (A) and Z-PSL (B) isomers. The respective structures at the equilibrium are also given as inlays.

This hypothesis is also strengthened by the fact that a secondary region which shows a consistent increase in flexibility when interacting with the Z-PSL emerges around the 80th residue, i.e. in the disordered loop which is not interacting with the lipid membrane and is, in the full TIM-3, in contact with the mucin domain. Conversely, the CC' (residues 42-45) and the C'C'' (residues 65-70) loops become slightly less flexible when the IvG domain is interacting with the Z-PSL.

Finally, in order to fully characterize the binding of the two isomers to the IvG domain, we report

the PMF along the distance between the center of mass of the PDS residues and the main binding pocket residues (see ESI) for the two isomers (Figure 5). Unexpectedly, the E-PSL profile is similar to that of the native lipids, particularly with respect to the equilibrium distance at 4.5 Å. Furthermore, the lipid binding proceeds barrierlessly, and the free energy profile is quite steep, suggesting that once bound, E-PSL resides stiffly in the binding pocket and explores a very limited conformational space. Interestingly, the free energy gain for the E-PSL isomer is even larger than that of the native lipid and amounts to around 30 kcal/mol. The Z-PSL isomer also shows a stable bound state corresponding to a global minimum in the free energy profile. Yet the minimum energy appears at larger distance from the binding pocket, 6.0 Å. More importantly the PMF profile is now noticeably shallower than for the E-isomers. The global free energy gain upon binding is also slightly reduced compared to the E isomers and is now reverted to about 25 kcal/mol. The broad PMF profile suggests that the Z isomer, most probably due to the steric clashes of the lipid tails and the azobenzene units, is now exploring a slightly wider conformational space and may reach larger distances. These results are in agreement withthe differences observed in the RMSF profile which shows a more pronounced flexibility for the IvG domain bound to the Z-PSL. The effects of the photoisomerization in shaping the interaction patterns of PSL lipids with the IvG domain of TIM-3 are, thus, evident even if rather modest. We may even hypothesize that the observed loss of activity of the protein is most probably due to the perturbation of the allosteric regulation, as a consequence of the alteration of the protein flexibility profile. The shallower PMF profile is also related to a broader and less tightly bound conformation which is again coherent with the modification of the protein global structural properties.

CONCLUSIONS.

We have performed long-range MD simulations of the IvG domain of TIM-3 in presence of a lipid bilayer exceeding the μs range and complemented with enhanced sampling. We have analyzed, at

a molecular level, the effect of the photoisomerization of modified lipids including an azobenzene moiety in shaping the activation of the innate immune system TIM-3 receptor. In particular, we haveshown that both isomers interact persistently in the protein binding pocket. Additionally, the interactions patterns are also similar to the ones developed by the native lipid. However, the Z-PSL conformation may induce some partial steric clashes between the lipid tails and the IvG domain of TIM-3. This, in turn, results in a more pronounced flexibility of the loops of the IvG domain, which may also disrupt the allosteric regulation of the protein and its activation in response to the interaction with phosphatidylserine lipids. These global observations are also confirmed by the PMF obtained at the umbrella sampling level. Indeed, the Z-PSL lipid exhibits a slightly larger distance from the center of the pocket and a shallower free energy profile, along with a slightly lower binding free energy compared to the E-PSL lipid. This observation may suggest that the larger conformational space visited by the Z-PSL lipid and the more important flexibility of the protein correlates with its loss of activity, in particular due to the perturbation of the allosteric network.

Our results establish the molecular bases underlying the activity of some recently proposed photoswitchable lipids as agents regulating TIM-3 activity in a context of photoimmunotherapy.

We also highlight how the perturbation caused by the photoisomerization of the proposed azobenzene-based lipids is globally modest, and hence can be insufficient to provide suitable therapeutic effects. Our work establishes the basis for the rational design of improved agents for photoimmunotherapy targeting TIM-3 and its IvG domain, aiming to increase its activity and selectivity. Modified lipids showing an improved regulation of TIM-3 will be presented in a forthcoming contribution.

ASSOCIATED CONTENT

Time series of the RMSD for the lipid bilayer and the IvG domain, individual RMSF for the IvG domain interacting with the E- and Z-PSL, interactions between the Ca^{2+} ion and the crucial protein residues, definition of the collective variable, distribution of the collective variable over the different windows, force field parameters for the isomerizable azobenzene unit. (file type, PDF)

AUTHOR INFORMATION

Corresponding Author

*Antonio.monari@u-paris.fr

Author Contributions

The manuscript was written through contributions of all authors. All authors have given approval to the final version of the manuscript.

ACKNOWLEDGMENT

The authors thank GENCI and Explor computing centers and the Platform P3MB for computational resources. A. M. thanks ANR and CGI for their financial support of this work

through Labex SEAM ANR 11 LABX 086, ANR 11 IDEX 05 02. The support of the IdEx "Université Paris 2019" ANR-18-IDEX-0001. Support from the Regional Development Fund of the European Union (Programme opérationnel FEDER-FSE Lorraine et Massif des Vosges 2014–2020/ "Fire Light" project: Photo-bio-active molecules and nanoparticles") for financial support.

REFERENCES

(1) Chaplin, D. D. Overview of the Immune Response. *Journal of Allergy and Clinical Immunology* **2010**, *125* (2), S3–S23. https://doi.org/10.1016/j.jaci.2009.12.980.

(2) Marshall, J. S.; Warrington, R.; Watson, W.; Kim, H. L. An Introduction to Immunology and Immunopathology. *Allergy, Asthma & Clinical Immunology* **2018**, *14* (S2), 49. https://doi.org/10.1186/s13223-018-0278-1.

(3) Pisetsky, D. S. Pathogenesis of Autoimmune Disease. *Nature Reviews Nephrology*. Nature Research August 1, 2023, pp 509–524. https://doi.org/10.1038/s41581-023-00720-1.

(4) Opferman, J. T. Apoptosis in the Development of the Immune System. *Cell Death Differ* **2008**, *15* (2), 234–242. https://doi.org/10.1038/sj.cdd.4402182.

(5) Sadler, A. J.; Williams, B. R. G. Interferon-Inducible Antiviral Effectors. *Nat Rev Immunol* **2008**, *8* (7), 559–568. https://doi.org/10.1038/nri2314.

(6) Gleason, M. K. M. K.; Lenvik, T. R. T. R.; McCullar, V.; Felices, M.; O'Brien, M. S. S.; Cooley, S. A. S. A.; Verneris, M. R. M. R.; Cichocki, F.; Holman, C. J. C. J.; Panoskaltsis-Mortari, A.; Niki, T.; Hirashima, M.; Blazar, B. R. B. R.; Miller, J. S. J. S. Tim-3 Is an Inducible Human Natural Killer (NK) Cell Receptor That Enhances Interferon Gamma Production in Response to Galectin-9 (GAL-9). *Biology of Blood and Marrow Transplantation* **2012**, *18* (2), S273. https://doi.org/10.1016/j.bbmt.2011.12.189.

(7) Bignon, E.; Marazzi, M.; Miclot, T.; Barone, G.; Monari, A. Specific Recognition of the 5′-Untranslated Region of West Nile Virus Genome by Human Innate Immune System. *Viruses* **2022**, *14* (6). https://doi.org/10.3390/v14061282.

(8) Bignon, E.; Miclot, T.; Terenzi, A.; Barone, G.; Monari, A. Structure of the 5′ Untranslated Region in SARS-CoV-2 Genome and Its Specific Recognition by Innate Immune System via the Human Oligoadenylate Synthase 1. *Chemical Communications* **2022**, *58* (13), 2176–2179. https://doi.org/10.1039/d1cc07006a.

(9) Chu, L.; Gong, Z.; Wang, W.; Han, G.-Z. Origin of the OAS–RNase L Innate Immune Pathway before the Rise of Jawed Vertebrates via Molecular Tinkering. *Proceedings of the National Academy of Sciences* **2023**, *120* (31). https://doi.org/10.1073/pnas.2304687120.

(10) Bhat, N.; Fitzgerald, K. A. Recognition of Cytosolic DNA by CGAS and Other STING-Dependent Sensors. *Eur J Immunol* **2014**, *44* (3), 634–640. https://doi.org/10.1002/eji.201344127.

(11) Morere, J.; Hognon, C.; Miclot, T.; Jiang, T.; Dumont, E.; Barone, G.; Monari, A.; Bignon, E. How Fragile We Are: Influence of Stimulator of Interferon Genes (STING) Variants on Pathogen Recognition and Immune Response Efficiency. *J Chem Inf Model* **2022**, *62* (12), 3096–3106. https://doi.org/10.1021/acs.jcim.2c00315.

(12) Freeman, G. J.; Casasnovas, J. M.; Umetsu, D. T.; Dekruyff, R. H. TIM Genes: A Family of Cell Surface Phosphatidylserine Receptors That Regulate Innate and Adaptive Immunity. *Immunol Rev* **2010**, *235* (1), 172–189. https://doi.org/10.1111/j.0105-2896.2010.00903.x.

(13) Chongsaritsinsuk, J.; Steigmeyer, A. D.; Mahoney, K. E.; Rosenfeld, M. A.; Lucas, T. M.; Smith, C. M.; Li, A.; Ince, D.; Kearns, F. L.; Battison, A. S.; Hollenhorst, M. A.; Judy Shon, D.; Tiemeyer, K. H.; Attah, V.; Kwon, C.; Bertozzi, C. R.; Ferracane, M. J.; Lemmon, M. A.; Amaro, R. E.; Malaker, S. A. Glycoproteomic Landscape and Structural Dynamics of TIM Family Immune Checkpoints Enabled by Mucinase SmE. *Nat Commun* **2023**, *14* (1), 6169. https://doi.org/10.1038/s41467-023-41756-y.

(14) Liu, Y.; Chen, H.; Chen, Z.; Qiu, J.; Pang, H.; Zhou, Z. Novel Roles of the Tim Family in Immune Regulation and Autoimmune Diseases. *Front Immunol* **2021**, *12*, 748787. https://doi.org/10.3389/fimmu.2021.748787.

(15) Weber, J. K.; Zhou, R. Phosphatidylserine-Induced Conformational Modulation of Immune Cell Exhaustion-Associated Receptor TIM3. *Sci Rep* **2017**, *7* (1), 13579. https://doi.org/10.1038/s41598-017-14064-x.

(16) Delova, A.; Pasc, A.; Monari, A. Interaction of the Immune System TIM-3 Protein with a Model Cellular Membrane Containing Phosphatidyl-Serine Lipids. *Chemistry – A European Journal* **2024**, *30* (22). https://doi.org/10.1002/chem.202304318.

(17) Kobayashi, N.; Karisola, P.; Peña-Cruz, V.; Dorfman, D. M.; Jinushi, M.; Umetsu, S. E.; Butte, M. J.; Nagumo, H.; Chernova, I.; Zhu, B.; Sharpe, A. H.; Ito, S.; Dranoff, G.; Kaplan, G. G.; Casasnovas, J. M.; Umetsu, D. T.; DeKruyff, R. H.; Freeman, G. J. TIM-1 and TIM-4 Glycoproteins Bind Phosphatidylserine and Mediate Uptake of Apoptotic Cells. *Immunity* **2007**, *27* (6), 927–940. https://doi.org/10.1016/j.immuni.2007.11.011.

(18) DeKruyff, R. H.; Bu, X.; Ballesteros, A.; Santiago, C.; Chim, Y.-L. E.; Lee, H.-H.; Karisola, P.; Pichavant, M.; Kaplan, G. G.; Umetsu, D. T.; Freeman, G. J.; Casasnovas, J. M. T Cell/Transmembrane, Ig, and Mucin-3 Allelic Variants Differentially Recognize Phosphatidylserine and Mediate Phagocytosis of Apoptotic Cells. *The Journal of Immunology* **2010**, *184* (4), 1918–1930. https://doi.org/10.4049/jimmunol.0903059.

(19) Santiago, C.; Ballesteros, A.; Martínez-Muñoz, L.; Mellado, M.; Kaplan, G. G.; Freeman, G. J.; Casasnovas, J. M. Structures of T Cell Immunoglobulin Mucin Protein 4 Show a Metal-Ion-Dependent Ligand Binding Site Where Phosphatidylserine Binds. *Immunity* **2007**, *27* (6), 941–951. https://doi.org/10.1016/j.immuni.2007.11.008.

(20) Huynh, M. L. N.; Fadok, V. A.; Henson, P. M. Phosphatidylserine-Dependent Ingestion of Apoptotic Cells Promotes TGF-B1 Secretion and the Resolution of Inflammation. *Journal of Clinical Investigation* **2002**, *109* (1), 41–50. https://doi.org/10.1172/JCI0211638.

(21) Sharma, B.; Kanwar, S. S. Phosphatidylserine: A Cancer Cell Targeting Biomarker. *Semin Cancer Biol* **2018**, *52*, 17–25. https://doi.org/10.1016/j.semcancer.2017.08.012.

(22) Nagata, S.; Suzuki, J.; Segawa, K.; Fujii, T. Exposure of Phosphatidylserine on the Cell Surface. *Cell Death Differ* **2016**, *23* (6), 952–961. https://doi.org/10.1038/cdd.2016.7.

(23) Naeini, M. B.; Bianconi, V.; Pirro, M.; Sahebkar, A. The Role of Phosphatidylserine Recognition Receptors in Multiple Biological Functions. *Cell Mol Biol Lett* **2020**, *25* (1), 23. https://doi.org/10.1186/s11658-020-00214-z.

(24) Kay, J. G.; Fairn, G. D. Distribution, Dynamics and Functional Roles of Phosphatidylserine within the Cell. *Cell Communication and Signaling* **2019**, *17* (1), 126. https://doi.org/10.1186/s12964-019-0438-z.

(25) Birge, R. B.; Boeltz, S.; Kumar, S.; Carlson, J.; Wanderley, J.; Calianese, D.; Barcinski, M.; Brekken, R. A.; Huang, X.; Hutchins, J. T.; Freimark, B.; Empig, C.; Mercer, J.; Schroit, A. J.; Schett, G.; Herrmann, M. Phosphatidylserine Is a Global Immunosuppressive Signal in Efferocytosis, Infectious Disease, and Cancer. *Cell Death Differ* **2016**, *23* (6), 962–978. https://doi.org/10.1038/cdd.2016.11.

(26) Wang, J.; Yu, C.; Zhuang, J.; Qi, W.; Jiang, J.; Liu, X.; Zhao, W.; Cao, Y.; Wu, H.; Qi, J.; Zhao, R. C. The Role of Phosphatidylserine on the Membrane in Immunity and Blood Coagulation. *Biomark Res* **2022**, *10* (1), 4. https://doi.org/10.1186/s40364-021-00346-0.

(27) Bevers, E. M.; Williamson, P. L. Getting to the Outer Leaflet: Physiology of Phosphatidylserine Exposure at the Plasma Membrane. *Physiol Rev* **2016**, *96* (2), 605–645. https://doi.org/10.1152/physrev.00020.2015.

(28) Asano, K.; Miwa, M.; Miwa, K.; Hanayama, R.; Nagase, H.; Nagata, S.; Tanaka, M. Masking of Phosphatidylserine Inhibits Apoptotic Cell Engulfment and Induces Autoantibody Production in Mice. *Journal of Experimental Medicine* **2004**, *200* (4), 459–467. https://doi.org/10.1084/jem.20040342.

(29) Chakravarti, S.; Sabatos, C. A.; Xiao, S.; Illes, Z.; Cha, E. K.; Sobel, R. A.; Zheng, X. X.; Strom, T. B.; Kuchroo, V. K. Tim-2 Regulates T Helper Type 2 Responses and Autoimmunity. *Journal of Experimental Medicine* **2005**, *202* (3), 437–444. https://doi.org/10.1084/jem.20050308.

(30) Todorich, B.; Zhang, X.; Slagle-Webb, B.; Seaman, W. E.; Connor, J. R. Tim-2 Is the Receptor for H-Ferritin on Oligodendrocytes. *J Neurochem* **2008**, *107* (6), 1495–1505. https://doi.org/10.1111/j.1471-4159.2008.05678.x.

(31) Chen, T. T.; Li, L.; Chung, D. H.; Allen, C. D. C.; Torti, S. V.; Torti, F. M.; Cyster, J. G.; Chen, C. Y.; Brodsky, F. M.; Niemi, E. C.; Nakamura, M. C.; Seaman, W. E.; Daws, M. R. TIM-2 Is Expressed on B Cells and in Liver and Kidney and Is a Receptor for H-Ferritin

Endocytosis. *Journal of Experimental Medicine* **2005**, *202* (7), 955–965. https://doi.org/10.1084/jem.20042433.

(32) Zhang, Y.; Ma, C. J.; Wang, J. M.; Ji, X. J.; Wu, X. Y.; Moorman, J. P.; Yao, Z. Q. Tim-3 Regulates pro- and Anti-Inflammatory Cytokine Expression in Human CD14+ Monocytes. *J Leukoc Biol* **2011**, *91* (2), 189–196. https://doi.org/10.1189/jlb.1010591.

(33) Zhao, L.; Cheng, S.; Fan, L.; Zhang, B.; Xu, S. TIM-3: An Update on Immunotherapy. *Int Immunopharmacol* **2021**, *99*, 107933. https://doi.org/10.1016/j.intimp.2021.107933.

(34) Avery, L.; Filderman, J.; Szymczak-Workman, A. L.; Kane, L. P. Tim-3 Co-Stimulation Promotes Short-Lived Effector T Cells, Restricts Memory Precursors, and Is Dispensable for T Cell Exhaustion. *Proceedings of the National Academy of Sciences* **2018**, *115* (10), 2455–2460. https://doi.org/10.1073/pnas.1712107115.

(35) Mishra, M.; Yadav, M.; Kumar, S.; Kumar, R.; Sen, P. TIM-3 Increases the Abundance of Type-2 Dendritic Cells during Leishmania Donovani Infection by Enhancing IL-10 Production via STAT3. *Cell Death Dis* **2023**, *14* (5), 331. https://doi.org/10.1038/s41419-023-05848-3.

(36) Chen, Z. Q.; Yu, H.; Li, H. Y.; Shen, H. T.; Li, X.; Zhang, J. Y.; Zhang, Z. W.; Wang, Z.; Chen, G. Negative Regulation of Glial Tim-3 Inhibits the Secretion of Inflammatory Factors and Modulates Microglia to Antiinflammatory Phenotype after Experimental Intracerebral Hemorrhage in Rats. *CNS Neurosci Ther* **2019**, *25* (6), 674–684. https://doi.org/10.1111/cns.13100.

(37) Wang, S. C.; Cao, C. M.; Piao, H. L.; Li, Y. H.; Tao, Y.; Zhang, X. M.; Zhang, D.; Sun, C.; Zhu, R.; Wang, Y.; Yuan, M. M.; Li, D. J.; Du, M. R. Tim-3 Protects Decidual Stromal Cells from Toll-like Receptor-Mediated Apoptosis and Inflammatory Reactions and Promotes Th2 Bias at the Maternal-Fetal Interface. *Sci Rep* **2015**, *5*, 9013. https://doi.org/10.1038/srep09013.

(38) Wolf, Y.; Anderson, A. C.; Kuchroo, V. K. TIM3 Comes of Age as an Inhibitory Receptor. *Nat Rev Immunol* **2020**, *20* (3), 173–185. https://doi.org/10.1038/s41577-019-0224-6.

(39) Khalaf, S.; Toor, S. M.; Murshed, K.; Kurer, M. A.; Ahmed, A. A.; Abu Nada, M.; Elkord, E. Differential Expression of TIM-3 in Circulation and Tumor Microenvironment of Colorectal Cancer Patients. *Clinical Immunology* **2020**, *215*, 108429. https://doi.org/10.1016/j.clim.2020.108429.

(40) Kim, H. S.; Chang, C. Y.; Yoon, H. J.; Kim, K. S.; Koh, H. S.; Kim, S. S.; Lee, S. J.; Kane, L. P.; Park, E. J. Glial TIM-3 Modulates Immune Responses in the Brain Tumor Microenvironment. *Cancer Res* **2020**, *80* (9), 1833–1845. https://doi.org/10.1158/0008-5472.CAN-19-2834.

(41) Kozłowski, M.; Borzyszkowska, D.; Cymbaluk-Płoska, A. The Role of TIM-3 and LAG-3 in the Microenvironment and Immunotherapy of Ovarian Cancer. *Biomedicines* **2022**, *10* (11), 2826. https://doi.org/10.3390/biomedicines10112826.

(42) Banerjee, H.; Nieves-Rosado, H.; Kulkarni, A.; Murter, B.; McGrath, K. V.; Chandran, U. R.; Chang, A.; Szymczak-Workman, A. L.; Vujanovic, L.; Delgoffe, G. M.; Ferris, R. L.; Kane, L. P. Expression of Tim-3 Drives Phenotypic and Functional Changes in Treg Cells in Secondary Lymphoid Organs and the Tumor Microenvironment. *Cell Rep* **2021**, *36* (11), 109699. https://doi.org/10.1016/j.celrep.2021.109699.

(43) de Mello, R. A.; Zhu, J. H.; Iavelberg, J.; Potim, A. H.; Simonetti, D.; Júnior, J. A. S.; Castelo-Branco, P.; Pozza, D. H.; Tajima, C. C.; Tolia, M.; Antoniou, G. Current and Future Aspects of TIM-3 as Biomarker or as Potential Targeted in Non-Small Cell Lung Cancer Scope: Is There a Role in Clinical Practice? *Transl Lung Cancer Res* **2020**, *9* (6), 2311–2314. https://doi.org/10.21037/tlcr-20-625.

(44) Chen, F.; Chen, Q.; Zhong, L.; Zhao, Y. Prospects of TIM-3 as a Promising Diagnostic and Prognostic Biomarker for Cancer Patients. *Discov Med* **2021**, *31* (162), 15–20.

(45) Bailly, C.; Thuru, X.; Goossens, L.; Goossens, J. F. Soluble TIM-3 as a Biomarker of Progression and Therapeutic Response in Cancers and Other of Human Diseases. *Biochem Pharmacol* **2023**, *209*, 115445. https://doi.org/10.1016/j.bcp.2023.115445.

(46) Das, M.; Zhu, C.; Kuchroo, V. K. Tim-3 and Its Role in Regulating Anti-Tumor Immunity. *Immunol Rev* **2017**, *276* (1), 97–111. https://doi.org/10.1111/imr.12520.

(47) Ausejo-Mauleon, I.; Labiano, S.; de la Nava, D.; Laspidea, V.; Zalacain, M.; Marrodán, L.; García-Moure, M.; González-Huarriz, M.; Hervás-Corpión, I.; Dhandapani, L.; Vicent, S.; Collantes, M.; Peñuelas, I.; Becher, O. J.; Filbin, M. G.; Jiang, L.; Labelle, J.; de Biagi-Junior, C. A. O.; Nazarian, J.; Laternser, S.; Phoenix, T. N.; van der Lugt, J.; Kranendonk, M.; Hoogendijk, R.; Mueller, S.; De Andrea, C.; Anderson, A. C.; Guruceaga, E.; Koschmann, C.; Yadav, V. N.; Gállego Pérez-Larraya, J.; Patiño-García, A.; Pastor, F.; Alonso, M. M. TIM-3 Blockade in Diffuse Intrinsic Pontine Glioma Models Promotes Tumor Regression and Antitumor Immune Memory. *Cancer Cell* **2023**, *41* (11), 1911-1926.e8. https://doi.org/10.1016/j.ccell.2023.09.001.

(48) Acharya, N.; Sabatos-Peyton, C.; Anderson, A. C. Tim-3 Finds Its Place in the Cancer Immunotherapy Landscape. *J Immunother Cancer* **2020**, *8* (1), e000911. https://doi.org/10.1136/jitc-2020-000911.

(49) Gandhi, A. K.; Kim, W. M.; Sun, Z. Y. J.; Huang, Y. H.; Bonsor, D. A.; Sundberg, E. J.; Kondo, Y.; Wagner, G.; Kuchroo, V. K.; Petsko, G.; Blumberg, R. S. High Resolution X-Ray and NMR Structural Study of Human T-Cell Immunoglobulin and Mucin Domain Containing Protein-3. *Sci Rep* **2018**, *8* (1), 17512. https://doi.org/10.1038/s41598-018-35754-0.

(50) Cao, E.; Zang, X.; Ramagopal, U. A.; Mukhopadhaya, A.; Fedorov, A.; Fedorov, E.; Zencheck, W. D.; Lary, J. W.; Cole, J. L.; Deng, H.; Xiao, H.; DiLorenzo, T. P.; Allison, J. P.; Nathenson, S. G.; Almo, S. C. T Cell Immunoglobulin Mucin-3 Crystal Structure Reveals a Galectin-9-Independent Ligand-Binding Surface. *Immunity* **2007**, *26* (3), 311–321. https://doi.org/10.1016/j.immuni.2007.01.016.

(51) Yang, X.; Li, M.; Qin, X.; Tan, S.; Du, L.; Ma, C.; Li, M. Photophosphatidylserine Guides Natural Killer Cell Photoimmunotherapy *via* Tim-3. *J Am Chem Soc* **2022**, *144* (9), 3863–3874. https://doi.org/10.1021/jacs.1c11498.

(52) Bandara, H. M. D.; Burdette, S. C. Photoisomerization in Different Classes of Azobenzene. *Chemical Society Reviews*. March 7, 2012, pp 1809–1825. https://doi.org/10.1039/c1cs15179g.

(53) Tiberio, G.; Muccioli, L.; Berardi, R.; Zannoni, C. How Does the Trans-Cis Photoisomerization of Azobenzene Take Place in Organic Solvents? *ChemPhysChem* **2010**, *11* (5), 1018–1028. https://doi.org/10.1002/cphc.200900652.

(54) Marvin Sketch 6.2.1, ChemAxon Ltd, Budapest, Hungary, URL: Http://Www.Chemaxon.Com. Paris.

(55) M. J. Frisch; G. W. Trucks; H. B. Schlegel; G. E. Scuseria; M. A. Robb; J. R. Cheeseman; G. Scalmani; V. Barone; G. A. Petersson; H. Nakatsuji; X. Li; M. Caricato; A. V. Marenich; J. Bloino; B. G. Janesko; R. Gomperts; B. Mennucci; H. P. Hratchian; J. V. Ortiz; A. F. Izmaylov; J. L. Sonnenberg; D. Williams-Young; F. Ding; F. Lipparini; F. Egidi; J. Goings; B. Peng; A. Petrone; T. Henderson; D. Ranasinghe; V. G. Zakrzewski; J. Gao; N. Rega; G. Zheng; W. Liang; M. Hada; M. Ehara; K. Toyota; R. Fukuda; J. Hasegawa; M. Ishida; T. Nakajima; Y. Honda; O. Kitao; H. Nakai; T. Vreven; K. Throssell; J. A. Montgomery; J. E. Peralta; F. Ogliaro; M. J. Bearpark; J. J. Heyd; E. N. Brothers; K. N. Kudin; V. N. Staroverov; T. A. Keith; R. Kobayashi; J. Normand; K. Raghavachari; A. P. Rendell; J. C. Burant; S. S. Iyengar; J. Tomasi; M. Cossi; J. M. Millam; M. Klene; C. Adamo; R. Cammi; J. W. Ochterski; R. L. Martin; K. Morokuma; O. Farkas; J. B. Foresman; D. J. Fox. Gaussian 16, Revision C.01, Gaussian, Inc., Wallingford CT, 2016. Revision C.01: Wallingford CT.

(56) D.A. Case; H.M. Aktulga; K. Belfon; I.Y. Ben-Shalom; J.T. Berryman; S.R. Brozell; D.S. Cerutti; T.E. Cheatham; G.A. Cisneros; V.W.D. Cruzeiro; T.A. Darden; R.E. Duke; G. Giambasu; M.K. Gilson; H. Gohlke; A.W. Goetz; R. Harris; S. Izadi; S.A. Izmailov; K. Kasavajhala; M.C. Kaymak; E. King; A. Kovalenko; T. Kurtzman; T.S. Lee; S. LeGrand; P. Li; C. Lin; J. Liu; T. Luchko; R. Luo; M. Machado; V. Man; M. Manathunga; K.M. Merz; Y. Miao; O. Mikhailovskii; G. Monard; H. Nguyen; K.A. O'Hearn; A. Onufriev; F. Pan; S. Pantano; A. Rahnamoun; D.R. Roe; A. Roitberg; C. Sagui; S. Schott-Verdugo; A. Shajan; J. Shen; C.L. Simmerling; N.R. Skrynnikov; J. Smith; J. Swails; R.C. Walker; J. Wang; H. Wei; R.M. Wolf; X. Wu; Y. Xiong; Y. Xue; D.M. York; S. Zhao; P.A. Kollman. AMBER 22, University of California, San Francisco. University of California, San Francisco.

(57) Knippenberg, S.; Osella, S. Push/Pull Effect as Driving Force for Different Optical Responses of Azobenzene in a Biological Environment. *The Journal of Physical Chemistry C* **2020**, *124* (15), 8310–8322. https://doi.org/10.1021/acs.jpcc.9b11391.

(58) Jo, S.; Kim, T.; Iyer, V. G.; Im, W. CHARMM-GUI: A Web-Based Graphical User Interface for CHARMM. *J Comput Chem* **2008**, *29* (11), 1859–1865. https://doi.org/10.1002/jcc.20945.

(59) Delova, A.; Pasc, A.; Monari, A. Interaction of the Immune System TIM-3 Protein with a Model Cellular Membrane Containing Phosphatidyl-Serine Lipids. *Chemistry – A European Journal* **2024**, *30* (22). https://doi.org/10.1002/chem.202304318.

(60) Freeman, G. J.; Casasnovas, J. M.; Umetsu, D. T.; Dekruyff, R. H. *TIM Genes: A Family of Cell Surface Phosphatidylserine Receptors That Regulate Innate and Adaptive Immunity*; 2010; Vol. 235.

(61) Dickson, C. J.; Madej, B. D.; Skjevik, Å. A.; Betz, R. M.; Teigen, K.; Gould, I. R.; Walker, R. C. Lipid14: The Amber Lipid Force Field. *J Chem Theory Comput* **2014**, *10* (2), 865–879. https://doi.org/10.1021/ct4010307.

(62) Mark, P.; Nilsson, L. Structure and Dynamics of the TIP3P, SPC, and SPC/E Water Models at 298 K. *Journal of Physical Chemistry A* **2001**, *105* (43), 9954–9960. https://doi.org/10.1021/jp003020w.

(63) Jorgensen, W. L.; Chandrasekhar, J.; Madura, J. D.; Impey, R. W.; Klein, M. L. Comparison of Simple Potential Functions for Simulating Liquid Water. *J Chem Phys* **1983**, *79* (2), 926–935. https://doi.org/10.1063/1.445869.

(64) Maier, J. A.; Martinez, C.; Kasavajhala, K.; Wickstrom, L.; Hauser, K. E.; Simmerling, C. Ff14SB: Improving the Accuracy of Protein Side Chain and Backbone Parameters from Ff99SB. *J Chem Theory Comput* **2015**, *11* (8), 3696–3713. https://doi.org/10.1021/acs.jctc.5b00255.

(65) Phillips, J. C.; Braun, R.; Wang, W.; Gumbart, J.; Tajkhorshid, E.; Villa, E.; Chipot, C.; Skeel, R. D.; Kalé, L.; Schulten, K. Scalable Molecular Dynamics with NAMD. *Journal of Computational Chemistry*. John Wiley and Sons Inc. 2005, pp 1781–1802. https://doi.org/10.1002/jcc.20289.

(66) Phillips, J. C.; Hardy, D. J.; Maia, J. D. C.; Stone, J. E.; Ribeiro, J. V.; Bernardi, R. C.; Buch, R.; Fiorin, G.; Hénin, J.; Jiang, W.; McGreevy, R.; Melo, M. C. R.; Radak, B. K.; Skeel, R. D.; Singharoy, A.; Wang, Y.; Roux, B.; Aksimentiev, A.; Luthey-Schulten, Z.; Kalé, L. V.; Schulten, K.; Chipot, C.; Tajkhorshid, E. Scalable Molecular Dynamics on CPU and GPU Architectures with NAMD. *Journal of Chemical Physics*. 2020. https://doi.org/10.1063/5.0014475.

(67) Humphrey, W.; Dalke, A.; Schulten, K. VMD: Visual Molecular Dynamics. *J Mol Graph* **1996**, *14* (1), 33–38. https://doi.org/10.1016/0263-7855(96)00018-5.

(68) Hopkins, C. W.; Le Grand, S.; Walker, R. C.; Roitberg, A. E. Long-Time-Step Molecular Dynamics through Hydrogen Mass Repartitioning. *J Chem Theory Comput* **2015**, *11* (4), 1864–1874. https://doi.org/10.1021/ct5010406.

(69) Miyamoto, S.; Kollman, P. A. Settle: An Analytical Version of the SHAKE and RATTLE Algorithm for Rigid Water Models. *J Comput Chem* **1992**, *13* (8), 952–962. https://doi.org/10.1002/jcc.540130805.

(70) Davidchack, R. L.; Handel, R.; Tretyakov, M. V. Langevin Thermostat for Rigid Body Dynamics. *J Chem Phys* **2009**, *130* (23). https://doi.org/10.1063/1.3149788.

(71) Feller, S. E.; Zhang, Y.; Pastor, R. W.; Brooks, B. R. Constant Pressure MolecularDynamics Simulation: The Langevin Piston Method. *J Chem Phys* **1995**, *103* (11), 4613– 4621. https://doi.org/10.1063/1.470648.

(72) Sargsyan, K.; Grauffel, C.; Lim, C. How Molecular Size Impacts RMSD Applications in Molecular Dynamics Simulations. *J Chem Theory Comput* **2017**, *13* (4), 1518–1524. https://doi.org/10.1021/acs.jctc.7b00028.

(73) Pitera, J. W. Expected Distributions of Root-Mean-Square Positional Deviations in Proteins. *J Phys Chem B* **2014**, *118* (24), 6526–6530. https://doi.org/10.1021/jp412776d.

(74) Kästner, J. Umbrella Sampling. *WIREs Computational Molecular Science* **2011**, *1* (6), 932–942. https://doi.org/10.1002/wcms.66.

(75) Grossfield, A. *An Implementation of WHAM: The Weighted Histogram Analysis Method Version 2.0.10*. http://membrane.